Filtering Properties of Hodgkin-Huxley Neuron to Different Time-Scale Signals

Dong Yu
Central China Normal University
Guowei Wang
Central China Normal University
Tianyu Li
Central China Normal University
Qianming Ding
Central China Normal University
Ya Jia (jiay@mail.ccnu.edu.cn)
Central China Normal University https://orcid.org/0000-0002-2818-9074

Research Article

Keywords: Neuronal filtering, Frequency selection, Hodgkin-Huxley neuron, Signal coding

Posted Date: November 12th, 2021

DOI: https://doi.org/10.21203/rs.3.rs-1041382/v1

Filtering properties of Hodgkin-Huxley neuron to different time-scale signals

Dong Yu, Guowei Wang, Tianyu Li, Qianming Ding, Ya Jia*

Department of Physics, Central China Normal University, Wuhan 430079, China

Abstract: Neuron can be excited and inhibited by filtered signals. The filtering properties of neural networks have a huge impact on memory, learning, and disease. In this paper, the filtering properties of Hodgkin–Huxley neuron to different time-scale signals are investigated. It is found that the neuronal filtering property depends on the locking relationship between the signal's frequency band and the natural frequency of neuron. The natural firing frequency is a combination of the fundamental component and the various level harmonic components. The response of neuron to the filtered signal is related to the amplitude of the harmonic components. Neuron responds better to the low−frequency signals than the high−frequency signals because of the reduction in the harmonic component amplitude. The filtering ability of neuron can be modulated by the excitation level, and is stronger around the excitation threshold. Our results might provide novel insights into the filtering properties of neural networks and guide the construction of artificial neural networks.

Keywords: Neuronal filtering · Frequency selection · Hodgkin–Huxley neuron · Signal coding

* Corresponding author: jiay@mail.ccnu.edu.cn

1. Introduction

Based on neuromathematical models, previous studies have explained complex neurodynamic problems [1, 2], helped to understand the human brain [3, 4], explained neural experiments [5–7]. In particular, neural network models have been used extensively in neuroscience applications, such as in studies of neural dynamics [8, 9], neural synchronization [10–14], information processing and transmission [15–17], and brain plasticity [18, 19], etc.

The effects of systemic parameters and external factors on the electrical activity of neural models have been widely investigated in previous works, such as the external current [20], time delay [21], synapses [22, 23], electric and magnetic fields [24, 25], patch temperature [26], ionic channel blockage [27, 28], various noises [29, 30], etc.. Some neurological diseases are correlated with pathological enhancement synchronization in neurons, such as Parkinsonism [31]. Therefore, suitable neuronal modeling is a critical approach to study complex neuronal electrical activity.

Noise [32], high–frequency signals [33], chaotic signals [34] can enhance neuronal response to weak signals. The phenomena of information transmission and detection have been studied in neural networks such as chain networks[35], small–world networks[36], feed–forward networks [37]. Therefore, it is of great importance to study signal processing in the neural system. Neurons are often subject to various signals, such as signals originating from different neurons and a single neuron but transmitted through different dendrites [38]. For example, Purkinje neurons gather thousands of excitatory and inhibitory synaptic inputs from the molecular layer and provide the sole output of the cerebellar cortex [7]. How such different time–scale signals are encoded and propagated in neural networks has significant implications for learning [39–41], memory [42, 43], and disease [44].

Previous studies [45] have investigated the filtering properties of neural networks to different time scales signals. Synapses function as dynamic filters for presynaptic spike sequences. Less important spikes are filtered out, and more important spikes are transmitted [46–48]. Similarly, synaptic failure is thought to be a means of gain control, whereby postsynaptic neurons can respond to important information from specific synapses, while filtering out less important inputs that reach other synapses [49, 50]. A synapse model with stochastic vesicle dynamics suppresses information encoded at lower than higher frequencies [51]. Refractoriness of vesicle recovery [52] and stochastic vesicle dynamics [51] alter the filtering properties of synapses. Short–term depressing and facilitating synapses transmit information best at low and high–frequencies, respectively [53]. Therefore the facilitated synapses are high pass filtered and serve as burst

detectors [47, 54, 55]. Cortical action potentials with higher frequencies were filtered more than those with lower frequencies [56, 57].

However, previous studies have reconstructed chemical synapse models to obtain synapses' filtering properties. Surprisingly little attention has been devoted to the filtering properties of the neuronal soma. Here we investigate the filtering properties of Hodgkin–Huxley (HH) neuron. The structure of this paper is as follows: in section 2, the mathematical model of HH are introduced. The main results are presented in section 3, and we summarize and discuss the potential implications of our findings in section 4.

2. Model

The temporal evolution of membrane potential of the HH [58] neuron model is described as follows:

$$C\frac{\mathrm{d}V}{\mathrm{d}t} = -G_K n^4 (V - E_K) - G_{Na} m^3 h (V - E_{Na}) - G_L (V - E_L) + I_0 + I_{\text{signal}}, \tag{1}$$

where V represents the membrane potential of the neuron, and $C = 1\ \mu\text{F/cm}^2$ is the capacity of the cell membrane. The reversal potentials for the potassium, sodium and leakage currents are $E_K = -77$ mV, $E_{Na} = 50$ mV, $E_L = -54.4$ mV, respectively. $G_K = 36\ \text{mS/cm}^2$, $G_{Na} = 120\ \text{mS/cm}^2$ and $G_L = 0.3\ \text{mS/cm}^2$ denote the maximum conductance of potassium, sodium and leakage currents, separately. The term I_0 is bias current which controls the excitability level of the neuron. The gating variables n, m and h, which characterize the average proportion of working channels opening obey the following Langevin equation:

$$\frac{\mathrm{d}y}{\mathrm{d}t} = \alpha_y (1 - y) - \beta_y y, \qquad (y = n, m, h) \tag{2}$$

where α_y and β_y are the switch rates of ionic channels which depend on voltage and described as follows:

$$\begin{cases} \alpha_n = \dfrac{0.01(V+55)}{1-\exp[-(V+55)/10]}, & \beta_n = 0.125\exp[-(V+65)/80], \\ \alpha_m = \dfrac{0.1(V+40)}{1-\exp[-(V+40)/10]}, & \beta_m = 4\exp[-(V+65)/80], \\ \alpha_h = 0.07\exp[-(V+65)/20], & \beta_h = \dfrac{1}{1+\exp[-(V+35)/10]}. \end{cases} \tag{3}$$

In Eq. (1), $I_{\text{signal}} = A(f)\sin(2\pi f\, t)$ is the external signal that is applied to HH neuron. f is the random frequency of the signal obtained from a computer–generated random number. The signal

can be seen as a combination of different time scale signals. As shown in Fig. 2(a), the signal's spectrum after the fast Fourier transform should be uniformly distributed. The amplitude in the external signal can be dependent on the frequency, and it is defined by [59]:

$$A(f)=\begin{cases}0, & f \geq f_{\max};\\ A_0, & f_{\min} \leq f \leq f_{\max};\\ 0, & f \leq f_{\min}.\end{cases} \tag{4}$$

According to the above definition, a filtered signal with a fixed frequency band can be obtained. A_0 is the amplitude of the filtered signal. The upper and lower threshold for frequency are defined by $f_{\max}$ and $f_{\min}$, respectively. We measure the mean firing rate r of HH neuron and record each spike when the membrane potential exceeded –20 mV:

$$r=\frac{1}{NT}\left(\sum_{j=1}^{N} n_{\text{spike},\,j}\right), \tag{5}$$

the term $n_{\text{spike},\,j}$ represents the spikes number of each realization j in the simulation time length T = 200 ms (i.e., 0.2 s), and M (M is set as 1000) means the times of realizations. The long time length is sufficient for the mean firing rate to satisfy the statistical law.

To precisely characterize the regularity of neural pulse signals, an appropriate measure of consistency, the coefficient of variation (CV) [60], is introduced, which is expressed as the ratio of standard deviation to average value

$$CV=\frac{\sqrt{\langle T^2\rangle-\langle T\rangle^2}}{\langle T\rangle}, \tag{6}$$

where $\langle T\rangle=\frac{1}{N}\sum_{i=1}^{N}(t_i-t_{i-1})$ represents the mean inter–spike intervals and $\langle T^2\rangle=\frac{1}{N}\sum_{i=1}^{N}(t_i-t_{i-1})^2$ represents the mean squared inter–spike interval. When CV reaches a minimum, it means that the pattern of neuron discharge is the most regular. We are more interested in how CV changes when it is small. Therefore, in the calculation, we set the threshold as CV_s = 2, and if $CV > CV_s$, CV is replaced by the value of the fixed point CV = 2; otherwise, CV remains the same.

3. Numerical results and discussion

Neurons exhibit different kinetic properties at different excitation levels. As shown in Fig. 1a, the neuron remains quiescent at I_0 less than 6.2. Immediately afterward, the Hopf bifurcation occurred, and the neuron was periodically discharged. Meanwhile, as the bias current increases, the neurons discharge at a greater frequency in Fig. 1b.

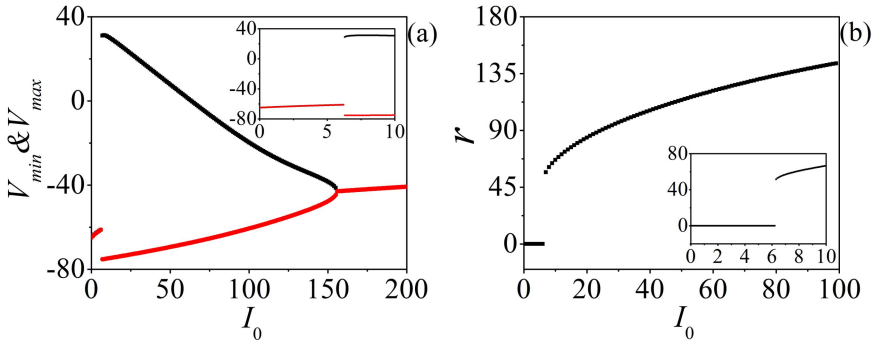

Fig. 1 a Bifurcation diagram of the Hodgkin–Huxley neuron. **b** Mean firing rate r dependence on the bias current I_0. The threshold bias current is $I_0 = 6.2$.

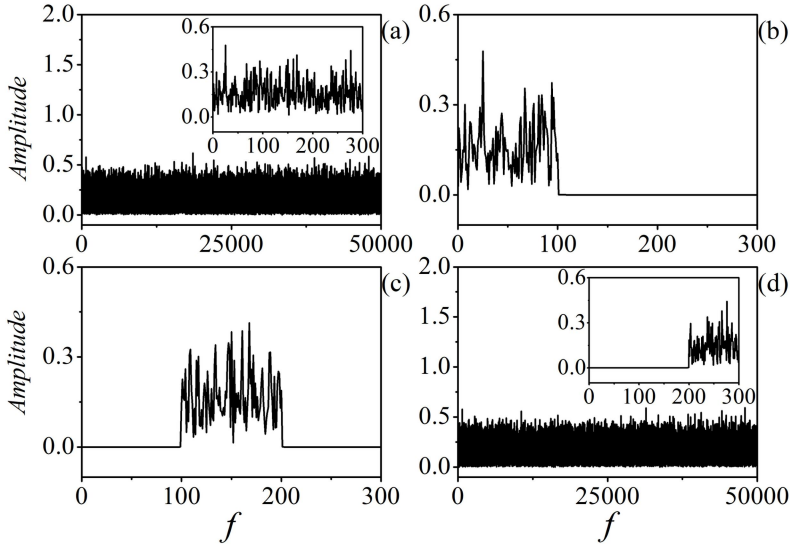

Fig. 2 a Spectrum of original signal after fast Fourier transform (FFT). The inserted sub–figure is an enlarged one within the region [0, 300]. Spectrum of the filtered signal after the FFT in the bands **b** $f_{min} = 0, f_{max} = 100$; **c** $f_{min} = 100, f_{max} = 200$; **d** $f_{min} = 200, f_{max} = \infty$. The inserted sub–figure is an enlarged one within the frequency region [0, 300]. The other parameters are fixed at $I_0 = 0, A_0 = 40$.

The external signals are filtered according to the criterion shown in Eq. (4), and the spectrum of original signals and after frequency selection are plotted in Fig. 2. That is, the thresholds f_{max}, f_{min} control the frequency band in the filtered signal. Therefore, external signals with different frequency bands can be obtained. Fig. 3a shows the temporal evolution of the filtered signal selected by different threshold values f_{max}, f_{min}. Note that the amplitude of the filtered signal is determined by the filter frequency bandwidth and the filtered signal amplitude. So the filtered

signal has a greater amplitude in Fig. 3a3.

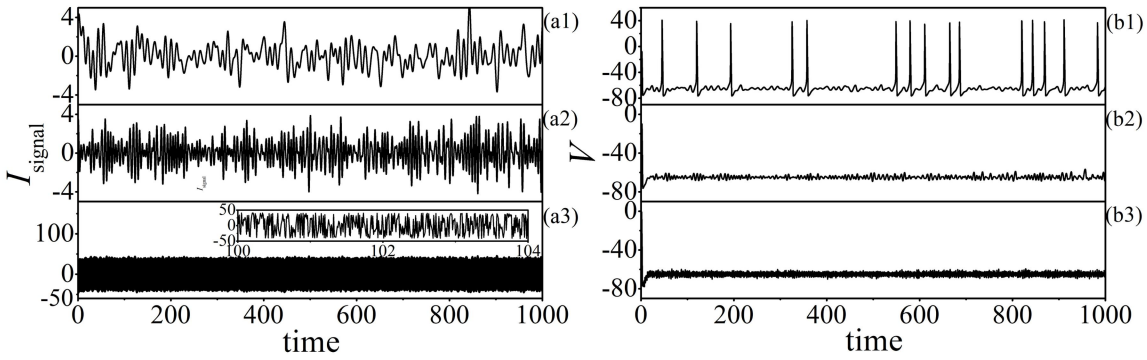

Fig. 3 Temporal evolution of external signal I_{signal} for different frequency bands: **a1** $f_{min} = 0$, $f_{max} = 100$; **a2** $f_{min} = 100$, $f_{max} = 200$; **a3** $f_{min} = 200$, $f_{max} = \infty$. The inserted sub–figure is an enlarged one within the time region [100, 104]. Temporal evolution of neuronal membrane potentials in different frequency bands of input: **b1** $f_{min} = 0$, $f_{max} = 100$; **b2** $f_{min} = 100$, $f_{max} = 200$; **b3** $f_{min} = 200$, $f_{max} = \infty$. The other parameters are fixed at $I_0 = 0$, $A_0 = 40$.

Fig. 3b shows the temporal evolution of the neuron's membrane potential, which applied different signals. The neural electrical activity is in the spike state in Fig. 3b1. It is in the quiescent state in Figs. 3b2 and b3. As shown in Fig. 1, the neuron transitions to a spiking state when the constant bias current is greater than 6.2. However, the amplitude of low–frequency band signal is close to 4 in Fig. 3b1, the neuron is spiking. The neuron is in a quiescent state when the amplitude of the high–frequency signal is close to 40 in Fig. 3b3. This suggests that neurons can filter complex signals from different time scales. Such filtering property is frequency dependent. Therefore the less important signals are filtered out, and more important signals are transmitted.

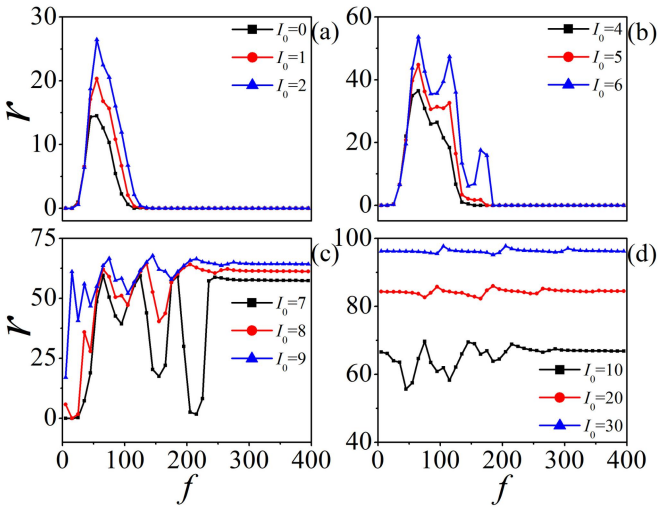

Fig. 4 The mean firing rate in response to frequency bands f for different bias current: **a** I_0 = 0–2; **b** I_0 = 4–6; **c** I_0 = 7–9; **d** I_0 = 10–30. The other parameters are fixed at $A_0 = 100$.

The excitation level of a neuron has a significant influence on its kinetic properties. It can be increased by tuning the bias current. To further study the relationship between neuronal filtering properties and excitation level, the mean firing rate as a function of the frequency band for different bias currents I_0 are shown in Fig. 4. Note that the frequency bandwidth is fixed at 10 HZ ($\Delta f = f_{max} - f_{min} = 10$HZ). The frequencies of the different data points in the curve represent the median of that frequency band interval. For example, the horizontal coordinate of the first point is 5HZ, which means that a 0–10HZ ($f_{min} = 0, f_{max} = 10$) signal is applied to the neuron. It is shown in Figs. 4a and b that the neuronal filtering range to filtered signals increases with increasing excitability levels. When the excitability of a neuron approaches a critical threshold (i.e., I_0 close to 6.2), the mean firing rate has a local maxima value in several specific frequency bands. However, neurons do not respond to high–frequency filtered signals. When I_0 is greater than 6.2, the neuron is in a spontaneous spike state. As a function of the frequency band, the mean firing rate demonstrates high and low in Figs. 4c and d. It suggests that the neuronal filtering properties are robust over different excitation levels.

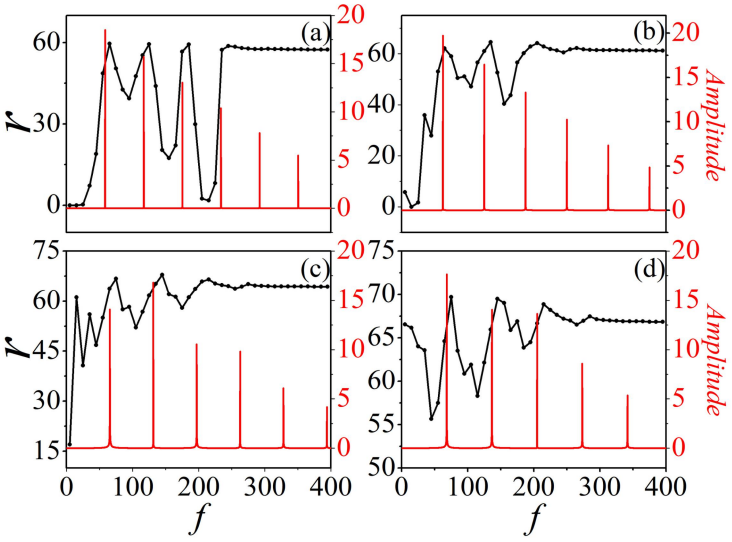

Fig. 5 The mean firing rate (black line) response to f and the spectrum (red line) of spontaneously firing neurons for different bias current: **a** $I_0 = 7$; **b** $I_0 = 8$; **c** $I_0 = 9$; **d** $I_0 = 10$. The other parameters are fixed at $A_0 = 100$.

According to the Fourier transform principle, the natural firing frequency of a neuron can be seen as a combination of the fundamental component and the various level harmonic components. The frequency of the fundamental component is equal to the natural firing frequency of the neuron. The mean firing rate of neurons shows interesting fluctuations in the low–frequency band.

It relates to the natural firing frequency of neurons. The mean firing rate as a function of frequency bands *f* (black line) and the spectrum of neuronal membrane potentials without filtered signal (red line) are shown in Fig. 5. It can be seen that the peaks of *r* correspond to the natural firing frequencies of the neuron. The neuronal excitation level is increased by the filtered signal. So the peak of the *r* curve is in the slightly higher frequency band of the natural oscillation frequency in Fig. 5. As the frequency band increases, the neuronal response to the signal continues to decrease as the harmonic amplitude decreases. Eventually, *r* does not fluctuate with changes in the high−frequency band signal. The above conclusions suggest that the filtering properties of the neuron are related to its natural frequency, responding to both fundamental and harmonic components of the natural firing. The degree of response depends on the amplitude of the harmonics components.

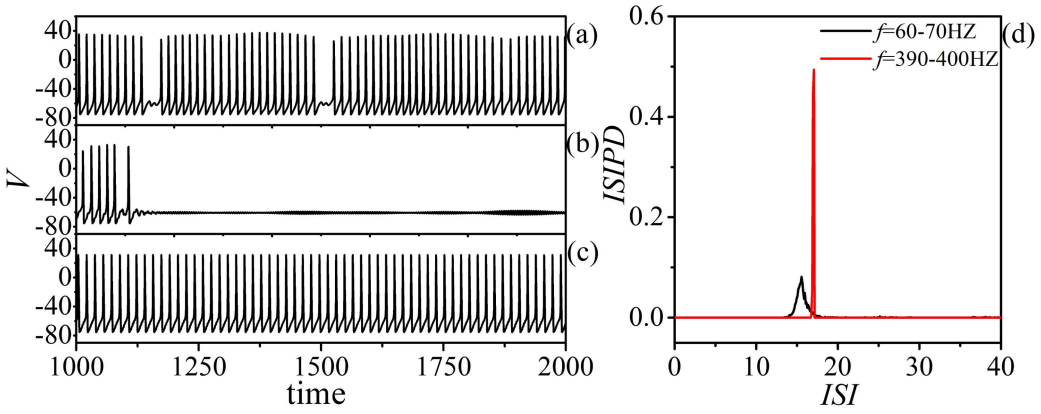

Fig. 6 Temporal evolution of neuronal membrane potentials in different frequency bands of input: **a** f_{min} = 60HZ, f_{max} = 70HZ; **b** f_{min} = 210HZ, f_{max} = 220HZ; **c** f_{min} = 390HZ, f_{max} = 400HZ. **d** The inter−spike interval (*ISI*) probability distribution (*ISIPD*) as a function of *ISI.* The other parameters are fixed at I_0 = 7, A_0 = 100.

However, the neurons responding to the fundamental component exhibit different kinetic properties from those affected by the high−frequency signal, even though the mean firing rates of the neurons are similar. In Figs. 6a−c, we have selected three specific points to study the spatio−temporal response of neurons to signals in different frequency bands (60−70, 210−220, 390−400HZ, respectively). Neuronal firing is suppressed for the frequency band between the two large amplitude harmonic components in Fig. 6b. Neurons responding to the fundamental component are in a multi−spike burst firing state in Fig. 6a. However, the neurons affected by high−frequency signals are in a regular spiking firing state in Fig. 6c. Analysis of inter−spike interval (*ISI*) probability distribution (*ISIPD*) revealed that the *ISI* is smaller and more divergent

by the effect of the low–frequency filtered signal. So neurons are more affected by low–frequency signals than high–frequency signals.

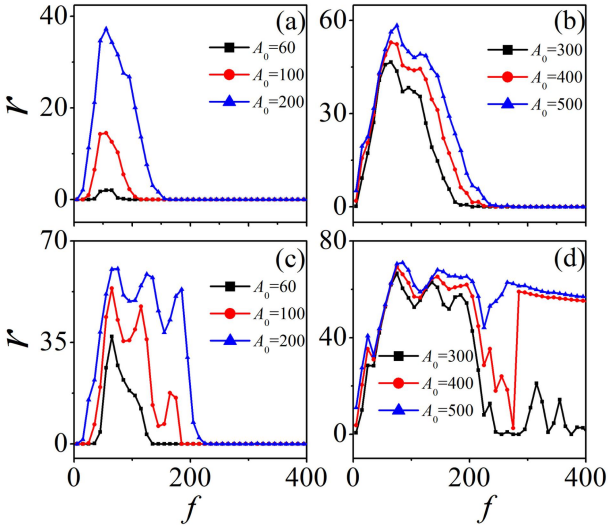

Fig. 7 The mean firing rate in response to frequency bands f for different A_0: **a** A_0 = 60–200 and **b** A_0 = 300–500 with I_0 = 0; **c** A_0 = 60–200 and **d** A_0 = 300–500 with I_0 = 6;

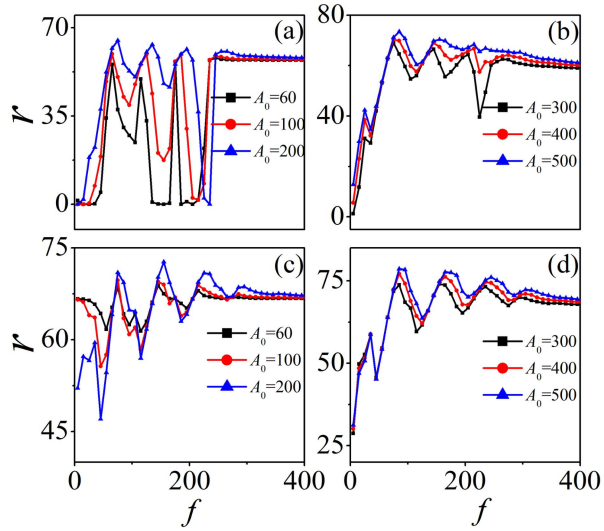

Fig. 8 The mean firing rate in response to frequency bands f for different A_0: **a** A_0 = 60–200 and **b** A_0 = 300–500 with I_0 = 7; **c** A_0 = 60–200 and **d** A_0 = 300–500 with I_0 = 10;

The mean firing rate as a function of frequency bands f for different A_0 are shown in Figs 7 and 8. For excitable neurons (I_0 < 6.2) with lower excitation levels (I_0 =0) in Figs 7a and b, it exhibits a lower response ability to harmonic components. As shown in Figs 7c and d, those with higher excitation levels respond best to harmonic components at moderate signal amplitudes (i.e., A_0 = 100, 200, 300). High–frequency signals with excessive amplitude (i.e., A_0 = 400, 500) increase neuronal excitability above the threshold, resulting in steady spontaneous firing. For

spontaneously firing neurons ($I_0 > 6.2$) in Fig. 8, neurons can respond to the harmonic component of the weak signal ($A_0 = 60$) in Figs. 8a and b, indicating a higher response ability to the harmonic component. Those with higher excitation levels in Figs. 8c and d can still respond to fundamental and harmonic components. However, fluctuations in the mean firing rate are suppressed, and the filtering ability is weakened. Therefore, the filtering ability of a neuron is modulated by its excitation level, with the best filtering ability near the excitation threshold.

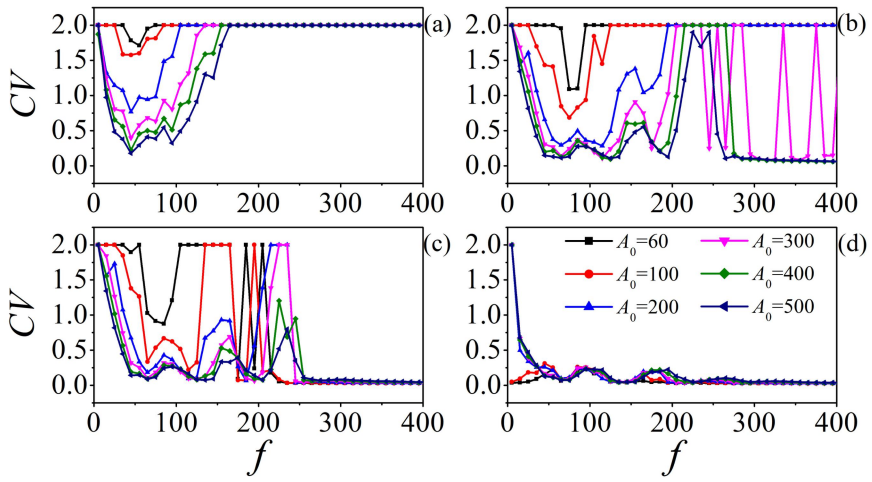

Fig. 9 Dependencies of CV on frequency bands f for different A_0: **a** $A_0 = 60–500$ with $I_0 = 0$; **b** $A_0 = 60–500$ with $I_0 = 6$; **c** $A_0 = 60–500$ with $I_0 = 7$; **d** $A_0 = 60–500$ with $I_0 = 10$; CV close to 2 indicates that the neuronal firing pattern is extremely irregular or quiescent. CV close to 0 indicates that the neuron get the best regular firing state.

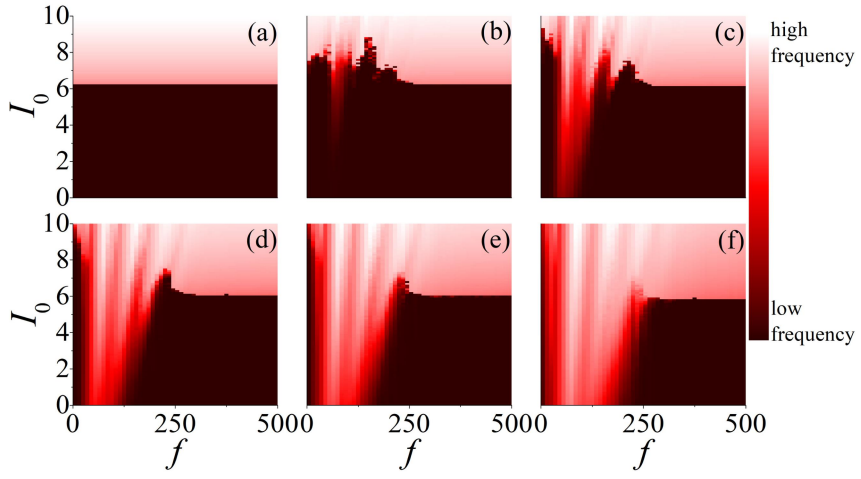

Fig. 10 Contour plots of mean firing rate r in the f–I_0 plane for different A_0: **a** $A_0 = 0$; **b** $A_0 = 40$; **c** $A_0 = 100$; **d** $A_0 = 200$; **e** $A_0 = 300$; **f** $A_0 = 500$.

By calculating the coefficient of variation, we identify the effect of the filtered signal on the regularity of neuronal firing patterns. The trend of the *CV* curve is almost opposite to the mean firing rate *r*. The excitable neuron in Fig. 9a is excited by a low–frequency signal so that firing regularity is increased. The neuron is not affected by the high–frequency signal, so the neuron remains quiescent, and the *CV* rises to 2. Neurons near the excitation threshold are more sensitive to filtered signals in Fig. 9b. Thus large amplitude signals behave like bias current, putting neuron in a regular high–frequency spiking state. For spontaneously firing neurons in Figs. 9c and d, the regularity of neuronal firing fluctuates only in the low–frequency band. While the high–frequency filtered signal has little effect on the system. This is consistent with the above findings.

To get a global view of how bias current affects the neuronal filtering properties, the contour plots of mean firing rate *r* in the $f - I_0$ plane are shown in Fig. 10. Note that the neuron still receives the same frequency bandwidth ($\Delta f = f_{max} - f_{min}$ = 10HZ) signal as in Figs. 4–9. For the regions where I_0 is less than 6.2, the red region increases with increasing amplitude, indicating that the neuron's filtering range increases. For the low–frequency region where I_0 is greater than 6.2, part of the region first decreases and increases with increasing amplitude. This suggests that the filtering properties of spontaneously firing neurons vary non–monotonically with increasing signal amplitude.

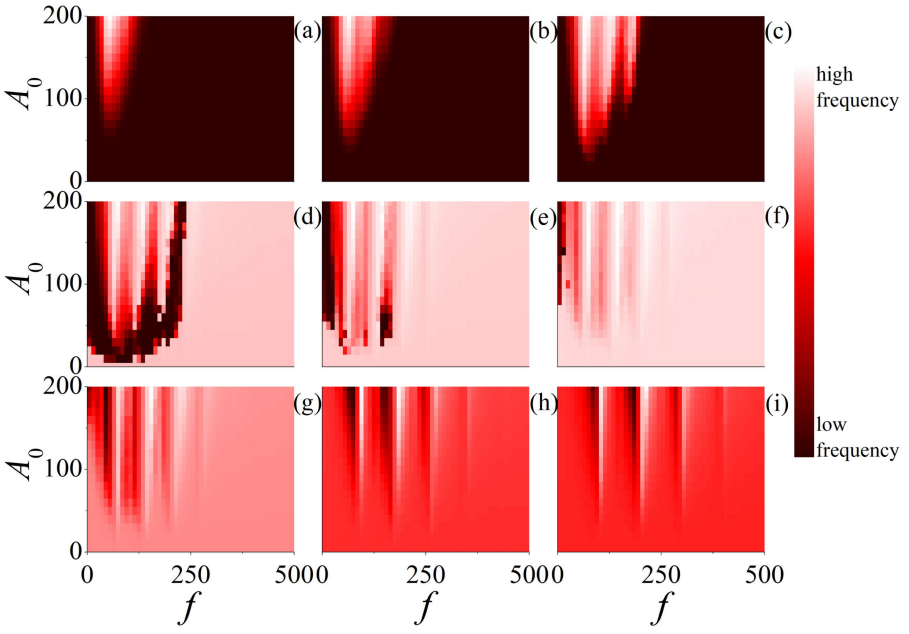

Fig. 11 Contour plots of mean firing rate *r* in the f–A_0 plane for different I_0: **a** $I_0 = 0$; **b** $I_0 = 3$; **c** $I_0 = 6$; **d** $I_0 = 7$; **e** $I_0 = 8$; **f** $I_0 = 9$; **g** $I_0 = 10$; **h** $I_0 = 20$; **i** $I_0 = 30$.

Further study of the contour plots of mean firing rate *r* in the f–A_0 plane found that its

filtering ability depends on the level of neuronal excitation. The red region increases with increasing bias current for excitable neurons in Figs. 11a–c. This suggests that the level of neuronal excitation enhances the filtering properties of the neuron. However, for spontaneously firing neurons in Figs. 11d–i, the neuron does not respond to high–frequency signals. Therefore there is a large area of the same colour in the high–frequency region. Dark regions decrease and regions of the same colour increase with increasing bias current. Which indicates that the excessive neuronal excitation level suppresses the filtering properties of the neuron for spontaneously firing neurons. In summary, the best filtering properties of neurons exist around the excitation threshold.

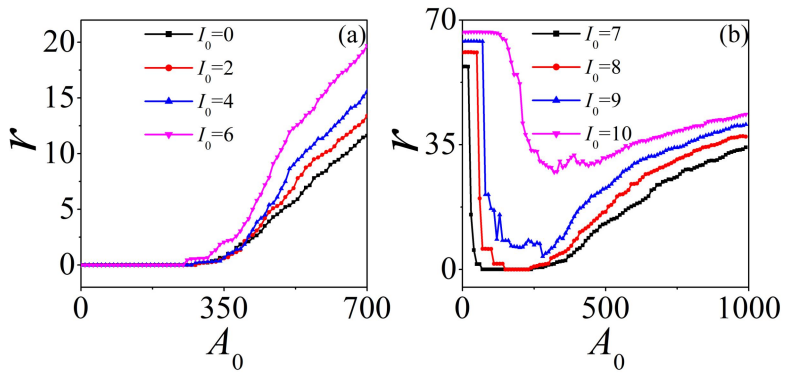

Fig. 12 The mean firing rate r in response to A_0 for different I_0: **a** I_0 = 0–6 and **b** I_0 = 7–10. f_{min} = 0, f_{max} = 10HZ.

We observe in Figs. 10 and 11 that the filtering properties of the neuron vary non–monotonically with increasing signal amplitude. In order to study the mechanism of the above phenomenon, the mean firing rate r as a function of A_0 are shown in Fig. 12. For excitable neurons in Fig. 12a, r increases monotonically with A_0. For spontaneously firing neurons in Fig. 12b, the mean firing rate is lowest for moderate signal amplitude values, which is the characteristic curve similar to the inverse stochastic resonance (ISR) [61]. A large number of previous works have illustrated that moderate noise levels can inhibit neuronal firing, a phenomenon known as ISR [62]. However, noise is a stochastic signal which contains multi–time scales. References [63] show that the inhibitory effect of colour noise on neurons is stronger than that of white noise. The spectrum of colour noise is non–uniformly distributed and has large amplitudes in specific frequency bands. This is similar to the filtered signal in the frequency domain. Thus, the ISR effects of colour noise on neurons may be similar to that of the inhibition of neurons by filtered signals. Both result from a mismatch between the frequency of the signal and the natural frequency of the neuron.

We plot the temporal evolution of neuronal membrane potentials at different excitation levels (i.e., I_0 = 7, 9, 10) in Fig. 13. As the signal amplitude increases, the electrical activities undergo a successive transition, i.e., spiking state → quiescent state or low–frequency spiking state → spiking state. This is consistent with the above conclusions. Our results are instrumental in investigating the effect of colour noise on ISR [61–65].

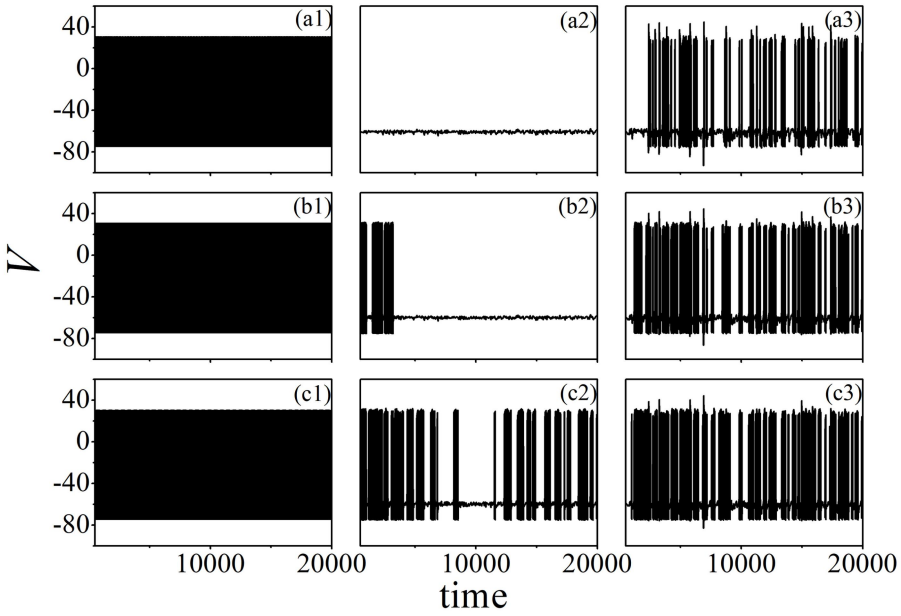

Fig. 13 Temporal evolution of neuronal membrane potentials. In the upper panel, I_0 = 7, **a1** A_0 = 0, **a2** A_0 = 200, **a3** A_0 = 600. In the middle panel, I_0 = 9, **b1** A_0 = 0,**b2** A_0 = 200, **b3** A_0 = 600. In the below panel, I_0 = 10, **c1** A_0 = 0, **c2** A_0 = 320, **c3** A_0 = 600. The frequency band is fixed at 0–10 HZ.

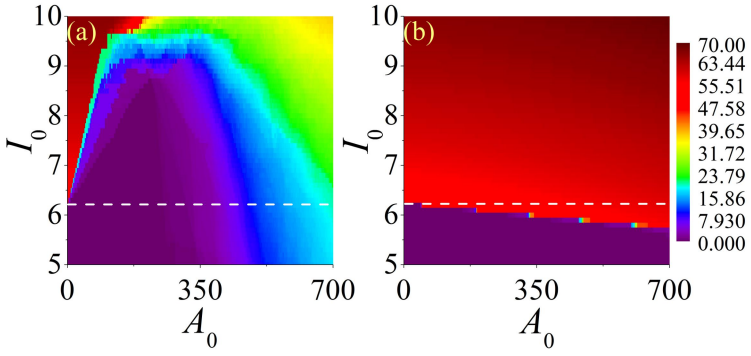

Fig. 14 Contour plots of mean firing rate r in the I_0–A_0 plane for different frequency bands f: **a** 0–10HZ; **b** 490–500HZ. The white dashed line separates the supra and sub–threshold bias currents.

To further globally compare the effects of high and low−frequency band filtered signals on neuronal firing patterns. The mean firing rate r in the I_0–A_0 plane are shown in Fig. 14. As neurons are applied with low−frequency signals in Fig. 14a, the ISR occurs over a large range of parameters. This means that moderately low−frequency signals inhibit neuronal firing. In contrast, the high−frequency signal has no region of ISR. Further analysis Fig. 14b revealed that the high−frequency signal behaves similarly to a bias current, promoting neuronal firing and reducing its excitation threshold.

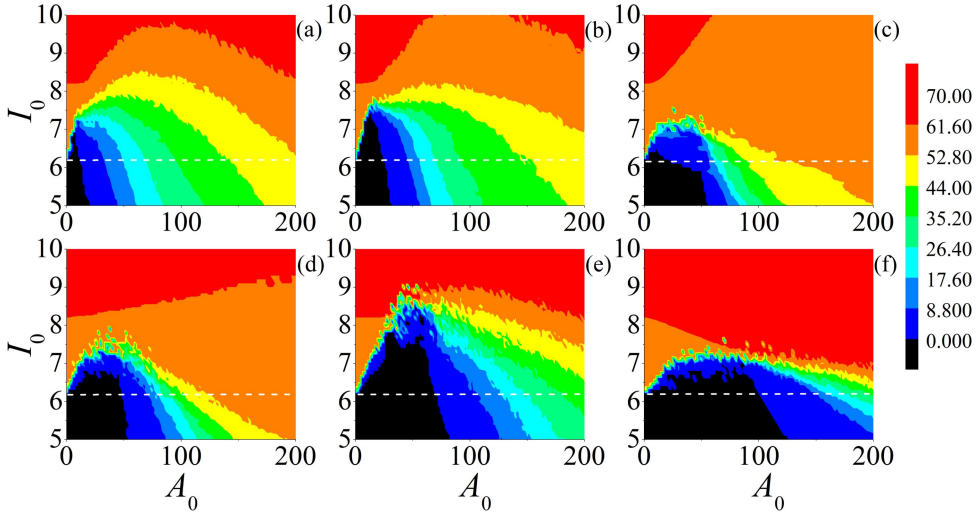

Fig. 15 Contour plots of mean firing rate r in the I_0–A_0 plane for different frequency bands f: **a** 70–80HZ; **b** 90–100HZ; **c** 110–120HZ; **d** 120–130HZ; **e** 150–160HZ; **f** 190–200HZ. The white dashed line separates the supra− and sub−threshold bias currents.

The signal filtering frequency band depends on the fundamental and harmonic components of spontaneous firing. Therefore, it is necessary to observe the neuronal response to signals in different frequency bands. As shown in Fig. 15, for excitable neurons, the firing threshold amplitude increases with increasing signal frequency. In contrast, for spontaneously firing neurons, the region of the inhibited region varies non−monotonically with increasing frequency. This suggests that excitable and spontaneously firing neurons obtain their filtering properties in two different ways.

4. Conclusions

Animals can detect signals with different frequency bands; for example, bats can detect

ultrahigh signals, while the human auditory system is sensitive to sounds within the frequency range of 20 to 20000 HZ [59]. In this paper, the filtering properties of HH neurons are investigated. Reliable wave filtering algorithms are proposed to obtain external signals with different frequency bands.

We found that a neuronal response to a signal is related to its natural firing frequency. For spontaneously firing neurons, signals consistent with harmonic frequencies enhance neuronal firing, while signals between harmonic frequencies inhibit neuronal firing. Neurons are virtually unaffected by high−frequency signals due to the reduction in harmonic amplitude. The filtering ability of neurons can be modulated by the excitation level and is stronger around the excitation threshold. When a neuron is subjected to a specific frequency band signal, the neuron's mean firing rate shows a characteristic curve of ISR as the signal intensity increases. Therefore, the filtering properties of neural networks are reflected in the synapses and the neuronal soma.

Further analysis revealed that the effects of low and high−frequency filtered signals play different roles in neuronal firing patterns. low−frequency signals inhibit neuronal firing, while high−frequencies behave like bias currents and excite neuronal firing. The responses of excitable and spontaneously firing neurons to filtered signals are not identical. The former has a firing threshold that increases monotonically with the signal’s frequency band, while the latter is related to the locking relationship between the harmonics and the signal.

We illustrate that the neuron is excited or inhibited by the filtered signal depending on the frequency locking relationship between the neuronal natural firing frequency and the signals' frequency band. However, we still have the unsolved problem of how to extract information about the filtered signal from a neuron. Thus, the mechanism of signal encoding and storage by neurons can be further understood. This is worthy of further study and discussion.

Acknowledgement

This project is supported by National Natural Science Foundation of China under Grants Nos 12175080 and 11775091.

Compliance with ethical standards

Data Availability Statement

All data generated or analysed during this study are included in this published article.

Conflict of interest

The authors declare that they have no potential conflict of interest.

References

1. Hou, Z.L., Ma, J., Zhan, X., et al.: Estimate the electrical activity in a neuron under depolarization field. Chaos, Solitons Fractals **142**, 110522 (2021)

2. Liu, Y., Ma, J., Xu, Y., et al.: Electrical mode transition of hybrid neuronal model induced by external stimulus and electromagnetic induction. Int. J. Bifurc. Chaos **29**, 1950156 (2019)

3. Antonopoulos, C.G., Srivastava, S., Pinto, S., et al.: Do Brain Networks Evolve by Maximizing Their Information Flow Capacity? PloS Comput. Biol. **11**, e1004372 (2015)

4. Roach, J.P., Sander, L.M., Zochowski, M.R.: Memory recall and spike−frequency adaptation. Phys. Rev. E **93**, 052307 (2016)

5. Enida, G., Friedemann, Z., Brice, B., et al.: Specific synaptic input strengths determine the computational properties of excitation inhibition integration in a sound localization circuit. J. Physiol. **596**, 4945–4967 (2018)

6. Enida, G., Clémentine, A., Sahlender, D.A., et al.: Ultrastructural basis of strong unitary inhibition in a binaural neuron. J. Physiol. **596**, 4969–4982 (2018)

7. Anatoly, B., Sarah R, Michael H, et al.: Inverse Stochastic Resonance in Cerebellar Purkinje Cells. PLoS Comput. Biol. **12**, e1005000 (2016)

8. Zhou, P., Yao, Z., Ma, J., et al.: A piezoelectric sensing neuron and resonance synchronization between auditory neurons under stimulus. Chaos, Solitons Fractals **145**, 110751 (2021)

9. Xu, Y., Guo, Y.Y., Ren, G.D., et al.: Dynamics and stochastic resonance in a thermosensitive neuron. Appl. Math. Comput. **385**, 125427 (2020)

10. Saha, A., Feudel, U.: Extreme events in FitzHugh−Nagumo oscillators coupled with two time delays. Phys. Rev. E **95**, 062219 (2017)

11. Belykh, I., Lange, E.D., Hasle, M.: Synchronization of Bursting Neurons: What Matters in the Network Topology. Phys. Rev. Lett. **94**, 188101 (2005)

12. Buric, N., Todorovic, K., Vasovic, N.: Synchronization of bursting neurons with delayed chemical synapses. Phys. Rev. E **78**, 036211 (2008)

13. Lu, L.L., Ge, M.Y., Xu, Y., et al.: Phase synchronization and mode transition induced by

multiple time delays and noises in coupled FitzHugh–Nagumo model. Physica A **535**, 122419 (2019)

14. Yu, D., Lu L.L., Wang, G.W., et al.: Synchronization mode transition induced by bounded noise in multiple time–delays coupled FitzHugh–Nagumo model. Chaos, Solitons Fractals **147**, 111000 (2021).

15. Wang Q.Y., Zhang, H.H., Chen, G.R.: Effect of the heterogeneous neuron and information transmission delay on stochastic resonance of neuronal networks. Chaos **22**, 219–R (2012)

16. Gan, C.B., Matjaz, P., Wang, Q.Y.: Delay–aided stochastic multi–resonances on scale–free FitzHugh–Nagumo neuronal networks. Chin. Phys. B **19**, 128−133 (2010)

17. Ge, M.Y., Jia, Y., Lu, L.L., et al.: Propagation characteristics of weak signal in feedforward Izhikevich neural networks. Nonlinear Dyn. **99**, 2355−2367 (2020).

18. Borges, R.R., Borges, F.S., Lameu, E.L., et al.: Spike timing–dependent plasticity induces non–trivial topology in the brain. Neural Networks **88**, 58−64 (2017)

19. Herholz, S.C., Zatorre, R.J.: Musical training as a framework for brain plasticity: behavior, function, and structure. Neuron **76**, 486−502 (2012)

20. Lu, L.L., Jia, Y., Xu, Y., et al.: Energy dependence on modes of electric activities of neuron driven by different external mixed signals under electromagnetic induction. Sci. China Technol. Sci. **62**, 427−440 (2019).

21. Soriano, M.C., Garsia–Ojalvo, J., Mirasso, C.R., et al.: Complex photonics: dynamics and applications of delay–coupled semiconductor lasers. Rev. Mod. Phys. **85**,421–470 (2013)

22. Lu, L.L., Jia, Y., Kirunda, J.B., et al.: Effects of noise and synaptic weight on propagation of subthreshold excitatory postsynaptic current signal in a feed–forward neural network. Nonlinear Dyn. **95**, 1673−1686 (2019).

23. Ge, M.Y., Jia, Y., Xu, Y., et al.: Wave propagation and synchronization induced by chemical autapse in chain Hindmarsh–Rose neural network. Appl. Math. Comput. **352**, 136−145 (2019).

24. Xu, Y., Jia, Y., Wang, H.W, et al.: Spiking activities in chain neural network driven by channel noise with field coupling. Nonlinear Dyn. **95**, 3237−3247(2019).

25. Xu, Y., Jia, Y., Kirunda, J.B., et al.: Dynamic behaviors in coupled neurons system with the excitatory and inhibitory autapse under electromagnetic induction. Complexity **2018**, 3012743 (2018).

26. Song, X.L, Wang, H.T., Chen, Y., et al.: Emergence of an optimal temperature in

429 action–potential propagation through myelinated axons. Phys. Rev. E **100**, 032416 (2019)
430 27. Zhou, X.Y., Xu, Y., Wang, G.W., et al.: Ionic channel blockage in stochastic Hodgkin–
431 Huxley neuronal model driven by multiple oscillatory signals. Cogn. Neurodyn. **14**, 569–578
432 (2020)
433 28. Xu, Y., Jia, Y., Ge, M.Y., et al.: Effects of ion channel blocks on electrical activity of
434 stochastic Hodgkin–Huxley neural network under electromagnetic induction. Neurocomputing
435 **283**, 196–204 (2018).
436 29. Yi, M., Jia, Y., Liu, Q., et al.: Enhancement of internal–noise coherence resonance by
437 modulation of external noise in a circadian oscillator. Phys. Rev. E **73**, 041923 (2006)
438 30. D'Onofrio A.: Bounded–noise–induced transitions in a tumor–immune system interplay.
439 Phys. Rev. E **81**, 021923 (2010)
440 31. Yu, Y., Wang, X.M., Wang, Q.S., et al.: A review of computational modeling and deep
441 brain stimulation:applications to Parkinson's disease. Appl. Math. Mech. **41**, 1747–1768 (2020)
442 32. Yao, Y.G., Ma, C.Z., Wang, C.J., et al.: Detection of sub–threshold periodic signal by
443 multiplicative and additive cross–correlated sine–Wiener noises in the FitzHugh–Nagumo
444 neuron. Physica A, **492**, 1247–1256 (2018)
445 33. Yang, L.J., Liu, W.H., Yi, M., et al.: Vibrational resonance induced by transition of
446 phase–locking modes in excitable systems. Phys. Rev. E **86**, 016209 (2012)
447 34. Baysal, V., Sara, Z., Yilmaz, E.: Chaotic resonance in Hodgkin–Huxley neuron.
448 Nonlinear Dyn. **97**, 1275–1285 (2019)
449 35. Ge, M.Y., Lu, L.L., Xu, Y., et al.: Vibrational mono–/bi–resonance and wave propagation
450 in FitzHugh–Nagumo neural systems under electromagnetic induction. Chaos, Solitons Fractals
451 **133**, 109645 (2020)
452 36. Baysal, V., Erdem, E., Yilmaz, E.: Impacts of autapse on chaotic resonance in single
453 neurons and small–world neuronal networks. Phil. Trans. R. Soc. A. **379**, 2198 (2021)
454 37. Diesmann, M., Gewaltig, M.O., Aertsen, A.: Stable propagation of synchronous spiking
455 in cortical neural networks. Nature **402**, 529–533 (1999)
456 38. Rosenbaum, R., Rubin, J., Doiron, B., et al.: Short Term Synaptic Depression Imposes a
457 Frequency Dependent Filter on Synaptic Information Transfer. PLoS Comput. Biol. **8**, e1002557
458 (2012)
459 39. Nguyen, P.V., Kandel, E.R.: Brief theta–burst stimulation induces a
460 transcription–dependent late phase of LTP requiring cAMP in area CA1 of the mouse

461 hippocampus. Learn. Memory **4**, 230–243 (1997)
462 40. Gyorgy B.: Theta oscillations in the hippocampus. Neuron **33**, 325–340 (2002)
463 41. Staubli, U., Lynch, G.: Stable hippocampal long–term potentiation elicited by 'theta'
464 pattern stimulation. Brain Res. **435**, 227–234 (1987)
465 42. Lamprecht, R., Ledoux, J.: Structural plasticity and memory. Nat. Rev. Neurosci. **5**,
466 45–54 (2004)
467 43. Nabavi, S., Fox, R., Proulx, C.D, et al.: Engineering a memory with LTD and LTP.
468 Nature **511**, 348 (2014)
469 44. Hensch, T.: Critical period plasticity in local cortical circuits. Nat. Rev. Neurosci. **6**,
470 877–888 (2005)
471 45. Bach, E.C., Kandler, K.: Long–term potentiation of glycinergic synapses by
472 semi–natural stimulation patterns during tonotopic map refinement. Sci. Rep. **10**, 16899 (2020)
473 46. Goldman, M.S., Maldonado, P., Abbott, L.F.: Redundancy Reduction and Sustained
474 Firing with Stochastic Depressing Synapses. J. Neurosci. **22**, 584–591 (2002)
475 47. Maass, W., Zador, A.M.: Dynamic Stochastic Synapses as Computational Units. Neural
476 Comput. **11**, 903 (1999)
477 48. Natschlager, T., Maass, W.: Computing the Optimally Fitted Spike Train for a Synapse.
478 Neural Comput. **13**, 2477–2494 (2001)
479 49. Goldman, M.S.: Enhancement of information transmission efficiency by synaptic
480 failures. Neural Comput. **16**, 1137 (2004)
481 50. Abbott, L.F., Varela, J.A., Sen, K., et al.: Synaptic Depression and Cortical Gain Control.
482 Science **275**, 221–224 (1997)
483 51. Rosenbaum, R., Rubin, J., Doiron, B., et al.: Short Term Synaptic Depression Imposes a
484 Frequency Dependent Filter on Synaptic Information Transfer. Plos Comput. **8**, e1002557 (2012)
485 52. Zucker, R.S., Regehr, W.G.: Short–term synaptic plasticity. Annu. Rev. Physiol. **64**,
486 355–405 (2002)
487 53. Galit, F., Idan, S., Henry, M., et al.: Coding of temporal information by
488 activity–dependent synapses. J. Neurophysiol. **87**, 140–148 (2002)
489 54. Lisman, J.E.: Bursts as a unit of neural information: making unreliable synapses reliable.
490 Trends Neurosci. **20**, 38–43 (1997)
491 55. Victor, M., Wang, X.J.: Differential Short–term Synaptic Plasticity and Transmission of
492 Complex Spike Trains: to Depress or to Facilitate? Cereb. Cortex **10**, 1143–1153 (2000)

56. Yu, Y.G, Shu, Y.S., Mccormick, D.A.: Cortical Action Potential Backpropagation Explains Spike Threshold Variability and Rapid–Onset Kinetics. J. Neurosci. **28**, 7260–7272 (2008)

57. Shu, Y.S, Hasenstaub, A., Duque, A., et al.: Modulation of intracortical synaptic potentials by presynaptic somatic membrane potential. Nature **441**, 761–765 (2006)

58. Hodgkin, A.L., Huxley, A.F.: The dual effect of membrane potential on sodium conductance in the giant axon of Loligo. J Physiol. **116**, 497–506 (1952)

59. Guo, Y.T., Zhou, P., Yao, Z. et al.: Biophysical mechanism of signal encoding in an auditory neuron. Nonlinear Dyn **105**, 3603–3614 (2021).

60. Schmid, G., Goychuk, I., Hanggi, P.: (2001) Stochastic resonance as a collective property of ion channel assemblies. Europhys. Lett. **56**, 22–28 (2001)

61. Lu, L.L., Jia, Y., Ge, M.Y., et al.: Inverse stochastic resonance in Hodgkin–Huxley neural system driven by Gaussian and non–Gaussian coloured noises. Nonlinear Dyn. **100**, 877–889 (2020)

62. Uzuntarla, M., Cressman, J.R, Ozer, M., et al.: Dynamical structure underlying inverse stochastic resonance and its implications. Phys. Rev. E **88**, 042712 (2013)

63. Guo, D.Q.: Inhibition of rhythmic spiking by coloured noise in neural systems. Cogn. Neurodyn. **5**, 293–300 (2011)

64. Huh, J.H.: Inverse stochastic resonance in electroconvection by multiplicative coloured noise. Phys. Rev. E **94**, 052702 (2016)

65. Uzuntarla, M., Torres, J.J., So, P., et al.: Double inverse stochastic resonance with dynamic synapses. Phys. Rev. E **95**, 012404 (2017)